AIAA JOURNAL
Vol. 34, No. 12, December 1996

Fountain Flows Produced by Multiple Impinging Jets in a Crossflow

Jorge M. M. Barata*
Universidade da Beira Interior, 6200 Covilhã, Portugal

A numerical and experimental study is made of the characteristics of vortex and upwash flows generated by multiple jets in a crossflow. Laser Doppler measurements and flow visualization are presented for turbulent circular jets emerging into a low-velocity cross stream and, then, impinging on a flat surface perpendicular to the geometrical jet nozzle axis. The experiments were performed for Reynolds numbers based on the jet exit conditions of 6×10^4 and 1.05×10^5, a jet-to-crossflow velocity ratio of 30, and an impinging height of 5 jet diameters, and they include mean and turbulent velocity characteristics along the two normal directions parallel to the nozzle axis. This study provides a basis to understanding more complex practical flowfields, such as those in industrial environments where impinging jets compete on any crosswind and the flow created underneath a vertical/short takeoff and landing aircraft. The results show the presence of a complex three-dimensional scarf vortex formed around each impinging jet and a fountain upwash flow resulting from the collision of the wall jets. In zones where measurements were not available, the flow details are numerically visualized using a solution of the time-averaged Navier–Stokes equations and the k-ε turbulence model.

Nomenclature

D = diameter of the jet
H = height of crossflow channel
k = turbulent kinetic energy
L = distance between the center of the jets along longitudinal direction
p = pressure
Re = Reynolds number
S = distance between the center of the jets along longitudinal direction
U = horizontal velocity, $\bar{U} + u'$
V = horizontal velocity, $\bar{V} + v'$
X = horizontal coordinate (positive in the direction of crossflow)
X_F = fountain origin
Y = vertical coordinate (positive in the direction of the jet flow)
Z = transverse coordinate (positive on the right side of the crossflow duct looking upstream)
ε = dissipation rate of k
ν_T = turbulent viscosity
σ_F = fountain inclination angle, 90 deg defined as vertical

Subscripts

F = upwash fountain flow
i = impingement
j = jet exit
o, ω = crossflow, ambient
p = penetration
s = stagnation
v = vortex

I. Introduction

TURBULENT jets impinging on flat surfaces through a low-velocity crossflow are typical in impingement cooling applications in industry, as well as of the flow beneath a vertical/short takeoff and landing aircraft, which is lifting off or landing with zero or small forward momentum. Ground effect may occur and change the lift forces on the aircraft, cause reingestion of exhaust gases into the engine intake, and raise fuselage skin temperatures. In this latter application, the impingement of each downward-directed jet on the ground results in the formation of a wall jet, which flows radially from the impinging point along the ground surface. The interaction of this wall jet with the freestream results in the formation of a scarf vortex far upstream of the impinging jet, which has profound implications on the aircraft design.[1,2] In addition, the collision of the wall jets originates a fountain upwash flow, affecting the forces and moments induced in the aircraft when operating in ground effect. Improved knowledge of impinging flows is therefore necessary to avoid these effects and to be able to model a range of jet-impingement types of applications with practical interest.

This paper presents a detailed analysis of the complex flowfield beneath multiple jets through a low-velocity crossflow and provides a quantitative picture of the main features of interest of impingement types of flows. The results include laser Doppler velocity measurements of flow characteristics, which are complemented by laser sheet visualization and extended to zones where information could not be successfully obtained, through numerical visualization based on the solution of the fully three-dimensional Reynolds-averaged Navier–Stokes equations incorporating an eddy viscosity model of turbulence.[3,4]

Earlier detailed measurements of the flow properties of fountain upwash are scarce and have been presented essentially in the absence of a crossflow and with the use of probe techniques. The most relevant works have been reviewed by Barata[5] and Saripalli[6] and indicated high turbulence levels and spreading rates in the fountains.[7–10] Kavasaoglu et al.[11] and Schetz et al.[12] also presented flowfield and pressure data for twin rectangular jets for small jet-to-crossflow velocity ratios (<10). Saripalli[6] reports laser Doppler velocity (LDV) measurements, including those of shear stress, for axisymmetric impinging jets with $S/D = 9$ and 14 and $H/D = 3$ and 5.5, but again the existence of a crossflow was not considered. Detailed measurements of the velocity characteristics of normal impinging jets on a flat surface can be more easily found for single jet configurations for relatively large impingement heights and normally for $H/D > 10$, using either probe and optical techniques, as reviewed, for example, by Barata[5] and Araújo et al.[13] Experiments on the aerodynamics of jets through a confined crossflow are much scarcer and have only been reported for large impingement heights and for low-velocity ratios between the jet and the crossflow V_j/U_o. These works have therefore only peripheral relevance to the vertical/short takeoff and landing (V/STOL) ground effect problem. Sugiyama

Presented as Paper 95-0190 at the AIAA 33rd Aerospace Sciences Meeting, Reno, NV, Jan. 9–12, 1995; received Jan. 10, 1995; revision received May 7, 1996; accepted for publication Aug. 22, 1996; also published in *AIAA Journal on Disc*, Volume 2, Number 1.

*Assistant Professor, Aeronautics Department, Rua Marquês d'Ávila e Bolama. Member AIAA.

and Usami,[14] Andreopoulos and Rodi,[15] and Shayesteh et al.[16] report hot-wire measurements for H/D ratios greater than 24 and for values of V_j/U_o, respectively, up to 1.95, 2, and 16. Kamotani and Greber[17] present results for $H/D = 12$, and Stoy and Ben-Haim[18] give pitot tube measurements for values of $H/D = 3.05$ and for jet-to-crossflow velocity ratios up to 6.8. Crabb et al.[19] report LDV measurements, including those of shear stress, but for values of $H/D = 12$ and for velocity ratios up to 2.3. Only Barata[5] provided detailed LDV measurements for a single jet configuration for a jet Reynolds number of $Re_j = 6 \times 10^4$, a velocity ratio between the jet and the crossflow of 30, 42, and 73 for the jet exit 3, 4, and 5 jet diameters above the ground plate. The measurements include time-resolved velocity characteristics along the horizontal and vertical directions, and respective correlations, in planes parallel to the jet nozzle axis. Part of this detailed experimental analysis has been reported by Barata et al.[20,21] The results are extended in the present work to multijet impinging configurations producing upwash fountain flows, which are the heart of the complicated effects by V/STOL aircraft when they operate in ground proximity.

Most of the published computational work on jets in crossflow are based on simplifying assumptions, which are capable of predicting global effects such as trajectories and jet cross-sectional shapes.[18,22,23] Patankar et al.[24] employed a finite difference numerical procedure together with a two-equation turbulence model to predict a single jet in a unconfined crossflow and obtained good agreement with the experiments of Keffer and Baines[22] and Ramsey and Goldstein[25] for velocity ratios from 2 to 10. A similar approach was used by Jones and McGuirk[26] to calculate the confined flow measured by Kamotani and Greber.[17] The gross features of the flow are well predicted, but the calculations appear to exhibit diffusion rates larger than those consistent with measured profiles, which can be attributed to the use of a first-order differencing scheme and very coarse meshes, making any statements on turbulence model accuracy impossible. Demuren[27] presented predictions of the flow measured by Sugiyama and Usami[14] using a three-dimensional finite difference scheme together with the k-ε turbulence model and found it necessary to adopt higher-order discretization schemes for the convection terms to obtain numerically accurate solutions. Barata et al.[28] and Barata[29] have also reported some numerical calculations for jet configurations relevant to the V/STOL problem providing an examination of the computational method based on their detailed measurements. The calculations presented in this paper follow those reported by Barata[29] and extend the analysis to the fountain flows and scarf vortex regions.

The remainder of this paper is presented in four sections. Section II describes the experimental configuration and measurement procedure. Section III describes the mathematical model, and Sec. IV presents the experimental results obtained in different planes parallel to the jet nozzle axis and quantifies the mean and turbulent velocity characteristics of the fountain upwash flows and scarf vortex. The calculation method is first evaluated against measurements in Sec. V, and then the present three-dimensional flows are numerically visualized. In addition, the location and penetration of the ground vortex are analyzed through pressure profiles obtained numerically. The final section summarizes the main findings and conclusions of this work.

II. Experimental Method

A. Flow Configuration

The experiments were carried out in a horizontal water channel, 1.50 m long and 0.5 m wide, made of perspex, as shown schematically in Fig. 1. The apparatus was built to allow multijet impingement experiments with variable impinging distances, H, but in the present study two and three jets of 20-mm exit diameter have been used at a fixed impingement height of 5 jet diameters.

The crossflow duct extends $20D$ upstream and $55D$ downstream of the central upstream jet. For the two-jets configuration the jets are separated by $5D$ and are located $10D$ from the nearest side wall. The third jet center was located at the symmetry plane $15D$ far upstream (see Fig. 1).

The origin of the horizontal X and vertical Y coordinates is taken at the center of the twin jets, in the upper wall of the tunnel: X is positive in the crossflow direction and Y is positive vertically downward.

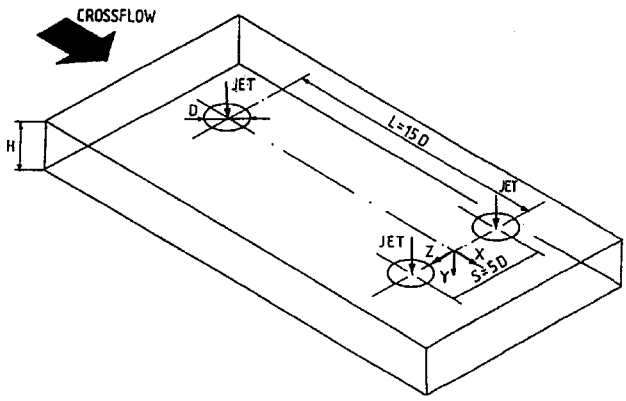

Fig. 1 Geometrical arrangement of the jets.

The transverse coordinate Z is taken as zero in the vertical plane of symmetry.

B. Experimental Techniques and Measurement Procedure

Flow visualization has been conducted by introducing a fluorescent dye into the jet and illuminating the central plane of the tunnel with a sheet of light obtained by spreading a laser beam.

A solution of fluorescein-sodium has been used and, in agreement with Saripalli,[30] found to be an ideal tracer fluid for the present application. The light source was a 1-W argon-ion laser in the 488-nm line, under which the fluorescein-sodium fluoresces a bright yellowish green. Visualization using air bubbles as tracer particles has also been performed using a similar illuminating system.

The velocity was measured by a dual-beam forward-scatter laser velocimeter, which comprised an argon-ion laser (514.5 nm; 1-W nominal power) and operated in the dual-beam, forward-scatter mode with sensivity of the flow direction provided by light frequency shifting from acousto-optic modulation (Bragg cells). The calculated half-angle of beam intersection in water was 3.48 deg, and the dimensions of the measuring volume at e^{-2} intensity were 2.225 and 0.135 mm.

The light scattered by naturally occurring centers in the water was collected by a lens (focal length of 150 mm) and focused into the pinhole aperture (0.3 mm) of a photomultiplier (EMI D136B) with a magnification of 0.76. The output of the photomultiplier was bandpass filtered, and the resulting signal processed by a laboratory-built frequency counter. Each measurement is subject to preset validations in the amplitude and time domains and, if valid, is digitized as a floating point number and transferred to a microcomputer.

The complete LDV system is mounted on a three-dimensional transversing unit, allowing the positioning of the laser velocimeter control volume within ± 0.5 mm. The horizontal U and vertical V mean velocity components and corresponding Reynolds shear stresses were determined from measurements with the laser beams in the horizontal and vertical planes and at ± 45 deg in the way described, for example, by Melling and Whitelaw.[31] To measure the vertical components in near-wall regions, the transmitting optics were inclined by half-angle of beam intersection, and the scattered light was collected off axis. Measurements could then be obtained up to 2 mm from the ground plate without a significant deterioration of the Doppler signals. Results obtained 20 mm above the ground plate with both the on-axis and the off-axis arrangements have shown a close agreement, within the precision of the equipment.

Errors incurred in the measurement of velocity by displacement and distortion of the measuring volume due to refraction on the duct walls and change in the refractive index were found to be negligibly small and within the accuracy of the measuring equipment. Nonturbulent Doppler broadening errors due to gradients of mean velocity across the measuring volume[32] may affect essentially the variance of the velocity fluctuations but for the present experimental conditions are on the order of $10^{-4} V_j^2$ and, therefore, sufficiently small for their effect to be neglected. The largest statistical (random) errors derived from populations of, at least, 10,000 velocity values were of 0.5 and 3%, respectively, for the mean and the variance values,

according to the analysis recommended by Yanta and Smith[33] for a 95% confidence interval.

Systematic errors incurred in the measurements of Reynolds shear stresses can arise from lack of accuracy in the orientation angle on the normal to the anemometer fringe pattern, as shown by Melling and Whitelaw[31] and can be particularly large in the vicinity of the zones characterized by zero shear stress: for the present experimental conditions the largest errors are expected to be smaller than −2.5%.

III. Mathematical Model

The numerical results presented are based on the solution of the fully three-dimensional form of the differential conservation equations for momentum and mass. Turbulence is modeled with the k-ε turbulence model.[34] The method is described in detail by Barata,[5] and only the main features are summarized here.

The solution of the governing equations was obtained using a finite difference formulation. The convection terms are evaluated using the QUICK scheme proposed by Leonard,[35] which is free from artificial diffusion and gives more accurate solutions than the hybrid scheme.

The solution procedure is based on the widely used SIMPLE algorithm and reported in the literature.[36]

The computational domain has six boundaries where the dependent variables are specified: an inlet and outlet plane and three solid walls at the top, bottom, and side of the channel. The sensitivity of the solutions to the location and outlet planes was investigated, and their final position is sufficiently far away from the jet so that the influence on the computed results is negligible. At the inlet boundary the profiles of all of the dependent variables are specified from the experimental results. At the outflow boundary the gradients of the dependent variables in the downstream direction are set to zero. On the symmetry plane the normal velocity vanishes, and the normal derivates of the other variables are zero. To overcome the requirement of very fine grids adjacent to walls in turbulent flow, wall functions are introduced to calculate quantities at grid points that are placed well outside of the viscous sublayer.[34] They take the form of expressions for the wall shear stress from which average production and dissipation of k across near-wall cell may be estimated. This method has become most popular[24,26] and has been applied to a large number of different flows with some success.[37]

IV. Results

The results presented in this section include flow visualization and detailed mean and turbulent velocity characteristics for the single-, two-, and three-jet flows.

The experimental program was performed in two stages. Prior to the detailed measurements, extensive visualization studies of the flow were performed to guide the choice of the measurement locations and to provide a qualitative picture of the flow. For all of the flows studied, the results have shown (for each jet) a pattern similar to that of a single impinging jet. Figure 2a identifies the flow development along the vertical plane of symmetry, i.e., $Z = 0$, and shows the initial potential-core jet region, where the flow characteristics are identical to those of a free jet, and the impingement region, characterized by considerable deflection of the jet after being slightly bent downstream by the pressure difference established across the jet. The deflected jet becomes almost parallel to the ground plate and exhibits a behavior similar to that of a radial wall jet where the upstream effects of interaction due to impingement are no longer important. The upstream wall jet interacts with the crossflow and forms a horseshoe vortex close to the ground plate, which wraps around the impinging jet like a scarf. As a result, two streamwise counterrotating vortices develop side to side and decay further downstream of the impinging zone. The nature of the flow is similar to the horseshoe structure known to be generated by the deflection of a boundary layer by a solid obstacle[38] but is different from the vortex pair known to exist in a bent-over jet in a crossflow far from the ground.[39] Analysis of Fig. 2 also suggests that the crossflow is deflected sideways by the penetration of the jet and may cause a recirculation region just downstream of the discharge, away from the ground plate. Figure 2c shows particle tracks or streaklines of the predicted velocity fields in the vertical plane of symmetry. The measured mean velocities, in

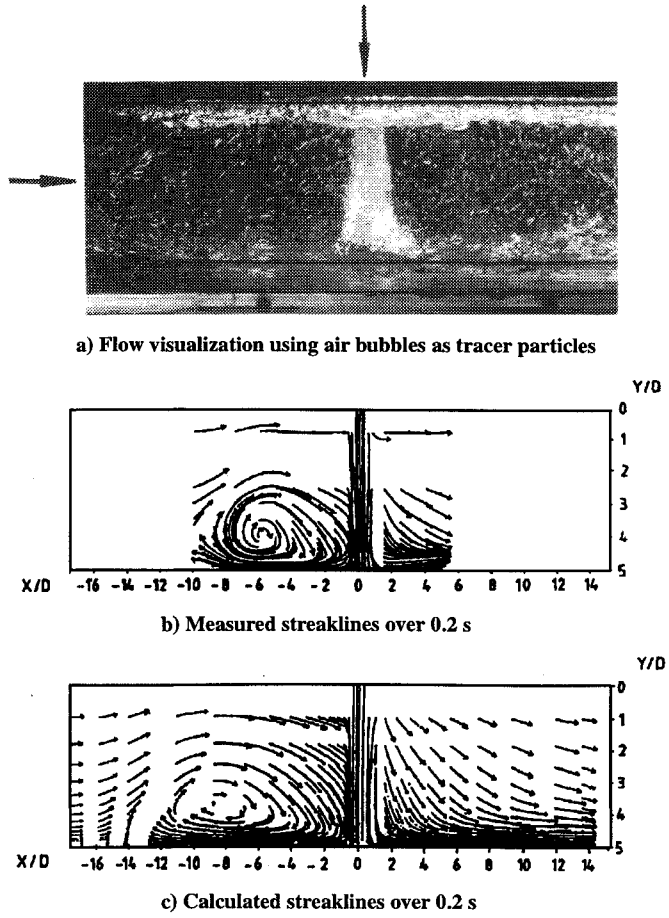

a) Flow visualization using air bubbles as tracer particles

b) Measured streaklines over 0.2 s

c) Calculated streaklines over 0.2 s

Fig. 2 Experimental and numerical visualization of the single-jet flow in the vertical plane of symmetry for $H/D = 5$ and $V_j/U_o = 30$.

the region of the same plane, have been fed into the same streakline plotting program to enable an easy comparison with the predictions and experimental visualization results. The simulations contain the gross features for the mean flow, although local differences do occur between measurements and calculations. The precise reason for these discrepancies is difficult to identify, because they may be attributed to numerical or turbulence modeling errors. However, the former were reduced by using the QUICK method and different meshes up to 180,000 nodes with nonuniform spacing, which allowed the achievement of grid independent solutions. On the other hand, modeling errors can be particularly large in the impinging zone due to limitations imposed by the turbulent viscosity hypothesis. Also, in the ground vortex region the numerical results can be influenced by the failure of the notion of the law of the wall at separation because the flow is no longer controlled by the wall shear stress.[40,41] Nevertheless, the jet trajectory is well predicted, and although the length of the recirculation zone associated with the ground vortex that wraps around the impinging jet is overpredicted, the gross features of the mean flow are well predicted. This suggests that the model is suitable to analyze the flow patterns that could not be readily observed in experiments, such as the structure of the ground vortex.

For the two-jet configuration an upwash fountain flow is formed in the center of the two impinging jets due to the collision of the two individual jets as shown in Fig. 3. Figures 3a and 3b identify the upwash flow in the vertical plane of symmetry and show that the upwash directions in this plane are asymmetric, because upstream of the jets the crossflow increases the angle of inclination with respect to the ground plane. Visualization of the flow in the transversal plane containing the center of the two jets has shown that the main jets are not strongly affected by the fountain. A considerable entrainment of surrounding fluid into the jets and fountain was also observed in the present experiments, but in contrast with the results of Saripalli[30] the upwash flow is asymmetric in relation to $X = 0$, in that the

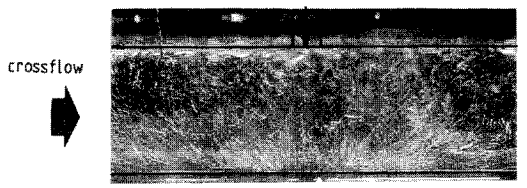

a) Flow visualization, two-jet case, $S/D = 5$

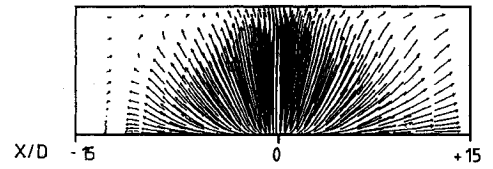

b) Calculated streaklines over 0.05 s (30 × 60 × 50 mesh), two-jet case, $S/D = 5$

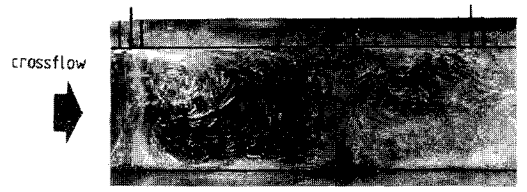

c) Flow visualization, three-jet case, $S/D = 5$ and $L/D = 15$

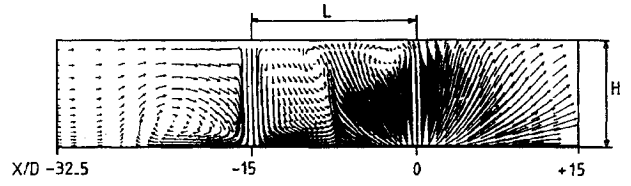

d) Calculated streaklines over 0.05 s (30 × 120 × 50 mesh), three-jet case, $S/D = 5$ and $L/D = 15$

Fig. 3 Experimental and numerical analysis of the fountain upwash flows in the vertical plane of symmetry for $Re_j = 1.05 \times 10^5$, $V_j/U_o = 30$, and $H/D = 5$.

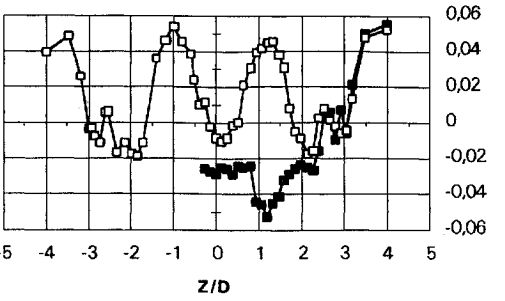

a) Mean horizontal velocity $\bar{U}/V_j$

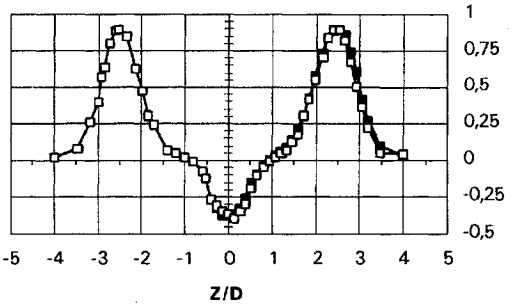

b) Mean vertical velocity $\bar{V}/V_j$

Fig. 4 Horizontal profiles of the velocity characteristics along the vertical transversal plane at $X = 0$ for $Y/D = 4$; $Re_j = 1.05 \times 10^5$, $V_j/U_o = 30$, $H/D = 5$, $S/D = 5$, and $L/D = 15$: □, two-jet case and ■, three-jet case.

crossflow lifts from the ground in the upstream part of the flow (i.e., for $X < 0$) in relation to that for $X > 0$.

In the absence of the crossflow, the wall jets are separated from each other along the ground plane by stagnation lines or dividing lines everywhere equidistant from the two-jet impingement centers, which contains a stagnation point.[42] In the present case the crossflow originates a second dividing line due to the collision of the wall jets and the crossflow. Near the symmetry plane this line is affected by the interference between the two ground vortexes due to the relatively small jet spacing ($S = 5D$).

Figures 3c and 3d show typical visualization of the flow along the vertical plane of symmetry for the three-jet configuration and identify the interaction between the fountain flow formed in the center of the two downstream impinging jets and the wall jet derived from the upstream impinging jet. This gives rise to an extended upwash fountain flow that is inclined due to the relative strengths of the upstream thin wall jet and the crossflow. The inclination of the central fountain as it leaves the ground plane with the X direction derived from Fig. 3c is $\sigma_F = 155$ deg. This is the same value obtained by Siclari et al.[42] for three-jet groups without the presence of a crossflow, using a theoretical method based on wall jet momentum equilibrium considerations. The value of σ_F corresponding to the present predictions (Fig. 3d) is about 90 deg, although the fountain inclination increases rapidly to 100 deg at a distance of $1D$ from its origin. Siclari et al.[42] use the same theory to estimate additional properties with interest in V/STOL: the fountain origin location and momentum. According to this theory, the fountain origin is located at $X/L = -0.5$, and its momentum is about 16% of the total jet momentum. The experiments show the origin of the fountain located further downstream at $X/L = -0.4$, revealing the influence of the crossflow, whereas the predictions give the value of $X/L = -0.5$. The confinement of the upwash flow and its interaction with the upstream impinging jet give rise to the recirculation shown in Fig. 3c downstream of the impinging jet, which is present in the calculations but located about $4D$ downstream.

The previous paragraphs have considered a qualitative analysis of the most salient features of the upwash flows considered in this paper. We now turn to the description of the detailed laser Doppler measurements of mean and turbulent velocities that quantify those features. The results are presented in the form of profiles obtained in the vertical plane crossing the center of the two off-center jets (i.e., $X = 0$) and in the longitudinal, vertical plane of symmetry (i.e., $Z = 0$) for the two- and three-jet configurations.

Figures 4a and 4b show the horizontal transversal profiles for axial $\bar{U}$ and vertical $\bar{V}$ mean velocity components for the two- and three-jet cases, for $Y/D = 4$, and quantify the development of the impinging jets and of the central fountain upwash flows. The measurements, and particularly those of the vertical component clearly identify for the two configurations a centrally located fountain rising from the ground plate without interference from the twin main jets, as it occurs in practical V/STOL applications.[43] This shows that the interjet spacing S used in the present experiments is large enough to avoid a sensible deflection of the jets perpendicular to the crossflow. The symmetry about the central plane at $Z = 0$ is also clearly demonstrated in Fig. 4 along the profile obtained for the two-jet configuration and reveals a precise matching of the jet exit velocities.

The initial profiles of the horizontal velocity $\bar{U}$ show peaks along the jet boundaries, which are considerably small in magnitude (about 0.4% of V_j) and may be associated with the transversal recirculatory flows originated by the central and lateral collisions of the wall jets. Note that the measurements obtained 2 mm downstream of the jet exit have established precise boundary conditions typical of a jet flow with a potential core and zero horizontal mean velocities. Based upon the detailed measurements of Barata et al.[28] for single impinging jets for $V_j/U_o = 30$, it is observed that the influence of the ground plate on the jet flows extend to about $3D$ above the plate, whereas the impinging zone is about $1D$ high. The maximum differences between the two- and the three-jet configurations are identified in the profiles of $\bar{U}$ and are explained by the influence of the front jet in the three-jet configuration.

The deflection of the impinging jets by the crossflow is identified by the negative values of $\bar{U}$ near the geometrical axis of the

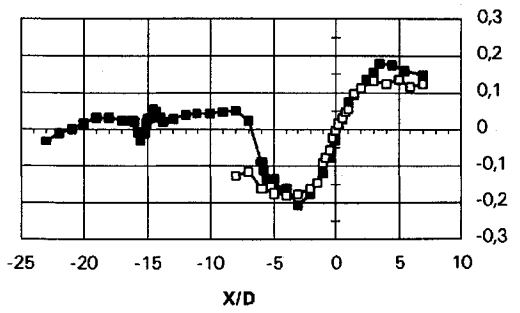

a) Mean horizontal velocity $\bar{U}/V_j$

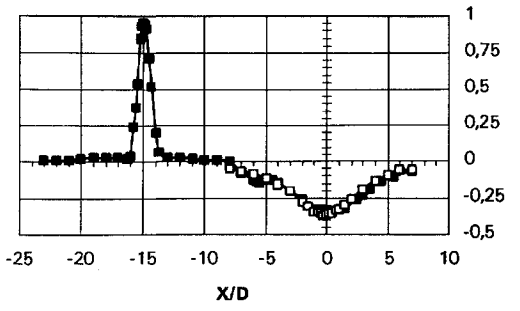

b) Mean vertical velocity $\bar{V}/V_j$

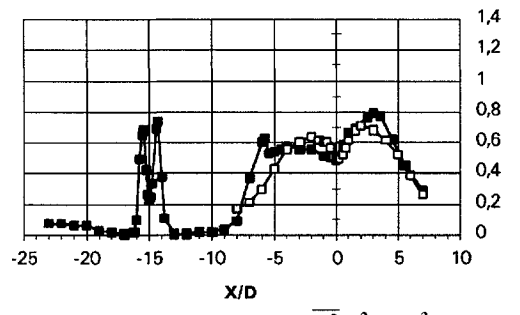

c) Horizontal normal stress $\overline{u'^2}/V_j^2 \times 10^3$

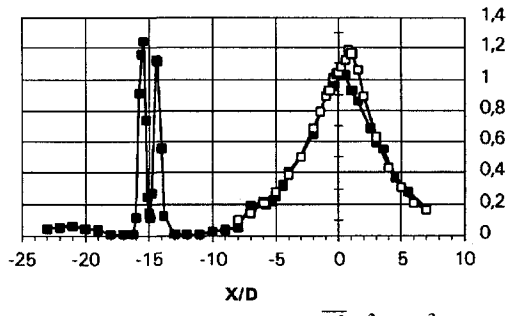

d) Vertical normal stress $\overline{v'^2}/V_j^2 \times 10^3$

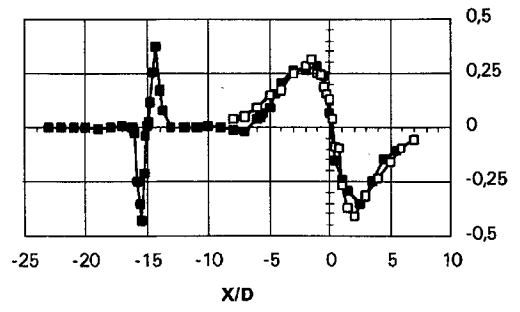

e) Reynolds shear stress $\overline{u'v'}/V_j^2 \times 10^3$

Fig. 5 Horizontal profiles of the velocity characteristics along the longitudinal plane of symmetry at $Z = 0$ for $Y/D = 4$; $Re_j = 1.05 \times 10^5$, $V_j/U_o = 30, H/D = 5, S/D = 5, L/D = 15$: □, two-jet case and ■, three-jet case.

jet exit, i.e., $Z/D = 0$. The negative values of $\bar{U}$ at the longitudinal plane of symmetry (i.e., $Z = 0$) are a consequence of the asymmetry along the crossflow direction of the fountain flow discussed earlier. These values also confirm that the central stagnation point of the upwash flow is displaced downstream by the crossflow, and in the case of the three-jet configuration the influence of the wall jet originated by the front jet is noted by the particularly high negative values of $\bar{U}$ and $Z/D = 1.2$ (about 5% of V_j).

The analysis of the upwash flows can be further documented with the help of Fig. 5, which shows horizontal profiles of velocity characteristics along the vertical plane of symmetry, for the two- and three-jet cases.

The distribution of the mean horizontal velocity $\bar{U}$ in the upwash flow region (i.e., around $X/D = 0$) is similar in both cases, although with increased asymmetries for the three-jet configuration. The mean horizontal velocity $\bar{U}$ increases in absolute magnitude at least up to $X/D = \pm 2.7$ and then decays.

The vertical velocities show maximum upward values around the central stagnation zone and decay monotonically to zero with X. For the two-jet configuration the distributions of the mean velocity components are asymmetric with respect to $X = 0$, with higher upward vertical velocities for $X < 0$. For the three-jet case the upwash flow is similar to that described previously, although with increased asymmetries. The interaction between the upstream wall jet and the upwash flow is identified between $X/D = -3$ and -7 with a plateau in the values of the upward vertical velocity between $X/D = -4$ and -6. Around $X/D = -15$, the profiles show features similar to those discussed by Barata et al.[28]

Figures 5c and 5d show the horizontal profiles along the vertical plane of symmetry for the normal stresses, for $Y/D = 4$, for the two- and three-jet configurations, revealing three regions of intense velocity fluctuations, namely, the shear layer surrounding the impinging jets, the impinging zones themselves, and the fountain upwash flow with maximum values similar to those found by Saripalli[6] for a two-jet impingement flow in the absence of a crossflow. These regions are characterized by the highest mean velocity gradients and are associated with near-Gaussian velocity probability distributions, suggesting the absence of discrete frequency oscillations. Figure 5e presents the distribution of the shear stress $\overline{u'v'}$, which away from the fountain upwash flow is similar to the results of Barata et al.[28] The impinging jets and the wall jets are dominated, respectively, by the mean strains $\partial\bar{V}/\partial X$ and $\partial\bar{U}/\partial Y$, and the sign of the shear stress is related with that of each shear strain in accordance with a turbulent viscosity hypothesis. Around the impinging point the two mean strains have the same order of magnitude and the thin shear layer approximation, as discussed by Castro and Bradshaw[44] and Bradshaw,[45] is no longer valid. The Reynolds shear stress decreases in the region of high stabilizing curvature typical of the impinging zones, reaching values of $\overline{u'v'}/V_j^2$ higher than those typical of well-behaved plane shear layers. Around the fountain flows the profiles of the Reynolds shear stress are consistent with the longitudinal asymmetry of the upwash and flow and, in general, with the direction of the mean flow. Around the stagnation point the shear stress is close to zero in the zones of zero shear strain, but the high turbulence levels measured may be explained by the interaction of normal stresses and normal strains.

V. Discussion

The detailed nature of the mean and fluctuating velocity measurements make the aforementioned data eminently suitable for validation of numerical models of the flow. The calculation method was first evaluated against LDV measurements obtained in the vicinity of the impingement zone for the single impinging jet case,[20] and then, having established a reasonable level of confidence in the mathematical model for the mean flow prediction, the present fountain flows calculations are presented.

Figure 6 shows horizontal profiles of $\bar{U}$ and $\bar{V}$, mean velocity components, and k estimated by $\frac{3}{4}(\overline{u'^2} + \overline{v'^2})$ along the longitudinal plane of symmetry ($Z = 0$) for the three-jet impinging case. The profiles of $\bar{U}$ and $\bar{V}$ (Figs. 6a and 6b) show a good agreement with the experiments in the impinging jet and upwash flows. The profiles of k (Fig. 6c) agree qualitatively with the experiments, but

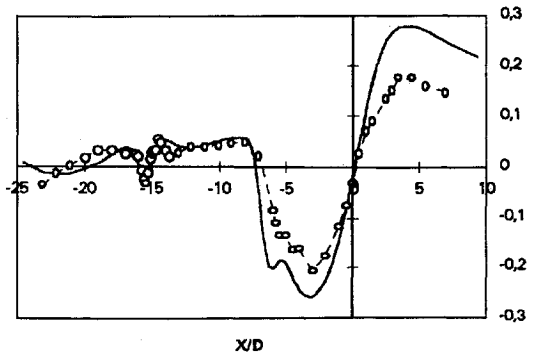

a) Mean horizontal velocity $\bar{U}/V_j$

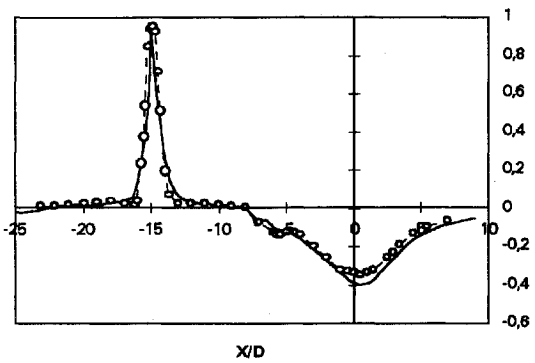

b) Mean vertical velocity $\bar{V}/V_j$

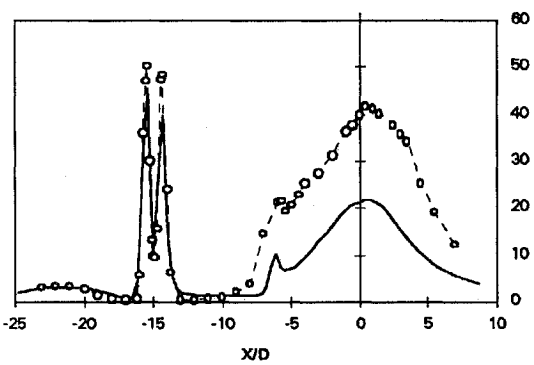

c) Turbulence kinetic energy $k/V_j^2 \times 10^3$

Fig. 6 Horizontal profiles of velocity characteristics along the longitudinal plane of symmetry for the three-jet configuration; $Re_j = 1.05 \times 10^5$, $V_j/U_o = 30$, $H/D = 5$, $S/D = 5$, and $L/D = 15$: ○, experiments and ——, predictions.

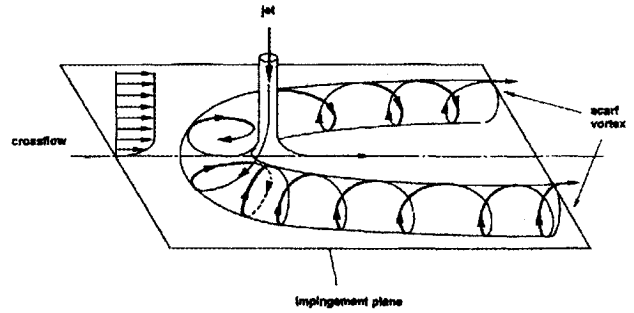

a) Perspective of the scarf vortex

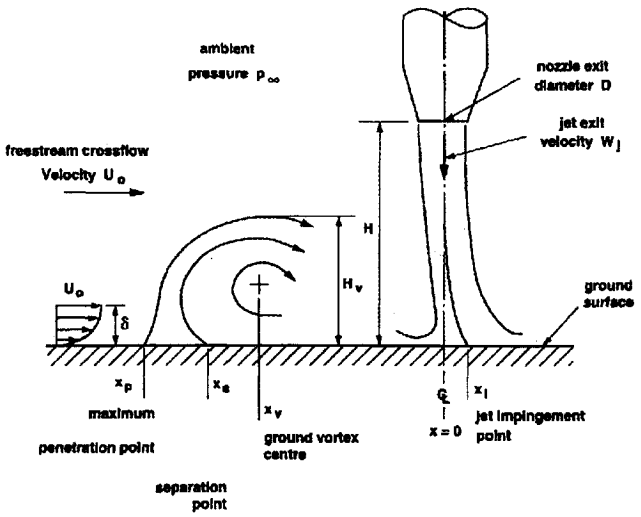

b) Plane of symmetry (i.e., Z = 0)

Fig. 7 Sketch of flow development for a jet impinging on a flat surface through a low-velocity crossflow at the vertical plane of symmetry (i.e., Z = 0).

the maximum values at the upwash are underpredicted, although far away from the ground plane, and for the twin-jet case, they could be well predicted. This grid refinement study allowed us to select the $19 \times 38 \times 31$ mesh and the $24 \times 92 \times 39$ mesh that give independent results for the two- and three-jet cases, respectively. To obtain a more accurate numerical visualization, the numerical results presented in this section were obtained using grids of $30 \times 60 \times 50$ and $30 \times 120 \times 50$ for the two- and three-jet cases, respectively.

The results of the previous section quantify the mean and turbulent velocity field typical of fountain flows produced by multiple impinging jets in a crossflow. For each impinging jet the results identify the formation of a ground vortex wrapped around each impinging jet due to the interaction of the forward flowing wall jet with the crossflow, in the way schematically shown in Fig. 7. As a consequence, two counter-rotating vortices trail away from each impinging zone and flow downstream in a way that is resembles a scarf. Knowles and Bray[2] demonstrated that much of the parametric work can be presented in terms of vortex penetration as a function of one of several parameters. Vortex penetration can be quantified by using X_P, where the maximum static pressure occurs, or X_S, corresponding to zero C_p. The most forward influence of the vortex is given by X_P and has consequently been used by several previous authors to quantify penetration. Another reason for its use is that smoke visualization gives a penetration that is close to this position.[2] On the other hand, oil film flow visualization will tend to show the separation position X_S, which is also more readily determined from ground pressure distributions, due to the shallow curvature that is often found near X_P.

Figure 8 shows calculated streaklines (particle trajectories) that complement the analysis of Sec. IV and offer insight into the nature of the fountain upwash flow and vortex structure formed around the impinging jet. For example, the streaklines of Fig. 8a show the wall jets[9] development near the impinging plane, revealing the stagnation line shapes, and together with the pressure distribution (Fig. 8b) quantify the complexity of the flow, identifying the presence of high- and low-pressure regions consistent with Fig. 8a. Figure 8b is a three-dimensional perspective of the pressure distribution at $Y/D = 3.8$ with a shape similar to the shape of the ground vortexes. An identical result was found by Barata et al.[1] for the case of single jets with a large low-pressure region resulting from the acceleration of the crossflow over the ground vortex.

Figure 9 presents predicted ground vortex static pressure distributions for the three configurations studied for $V_j/U_o = 30$. Figure 9a reveals a jet penetration of about $X_P = -14D$ for the single impinging jet case, whereas for the three-jet configuration it is difficult to identify the penetration of the front jet, which seems to be affected by the central upwash flow, giving rise to high static pressure values upstream $X/D = -10$. The ground vortex separation point is easily identified and assumes the values of $X/D = -8.5$ and -11 for the single- and three-jet cases. In contrast, no significant differences can be found for the ground vortex core position (minimum ground static pressure), which is about $X/D = -6.5$, revealing that the upwash flow in the case of the three-jet flow affects essentially the

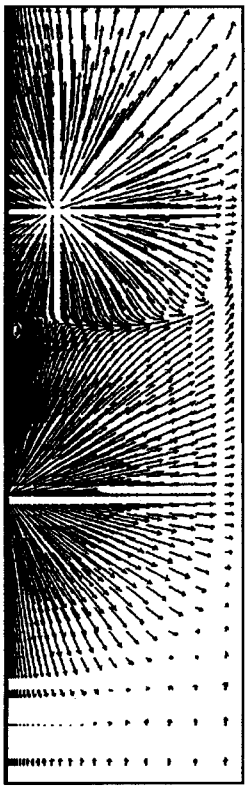

a) Calculated streaklines over 0.05 s along ground plane

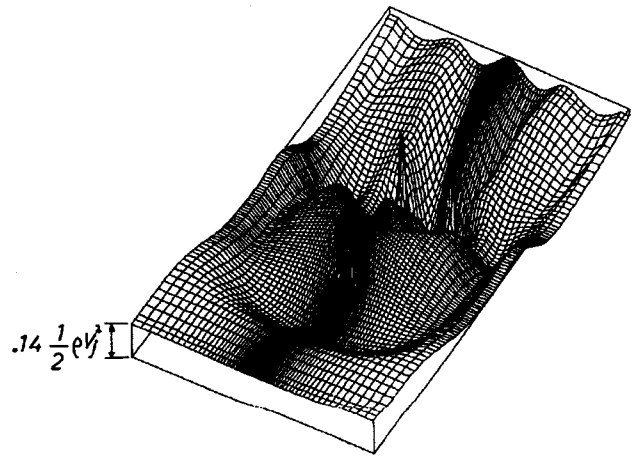

b) Three-dimensional perspective of pressure distribution in horizontal plane at $Y/D = 3.8$

Fig. 8 Numerical analysis of the fountain upwash flows for the three-jet configuration $Re_j = 1.05 \times 10^5$, $V_j/U_o = 30$, $H/D = 5$, $S/D = 5$, and $L/D = 15$.

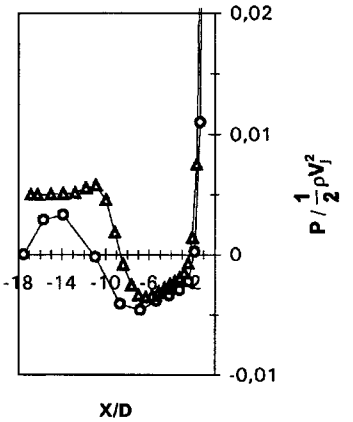

a) Vertical plane of symmetry (△: three-jet configuration; ○: single-jet configuration)

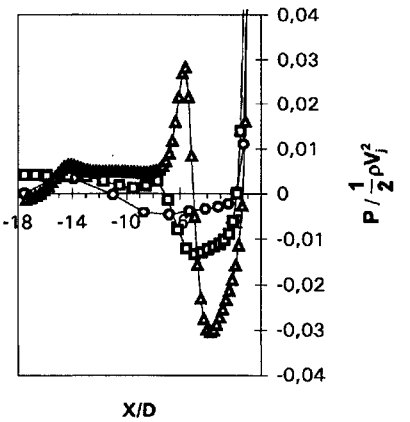

b) Vertical plane crossing the single (○) or a rear jet (□, two jets and △ three jets)

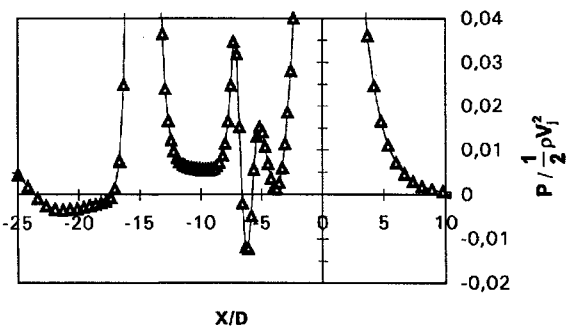

c) Upwash zone in the vertical plane of symmetry for the three-jet configuration

Fig. 9 Ground vortex static pressure distributions.

shape of the ground vortex, but its location is essentially dependent on the velocity ratio V_j/U_o.

Figure 9b compares the wall pressure distributions for the single and twin rear jets (two- or three-jet cases). For the twin-jet case, each jet penetration is reduced from $X/D = -14$ to -7.7, whereas the separation point and ground vortexes centers are displaced downstream by about $4D$. The pressure distribution crossing the center of the two rear jets for the three-jet configuration shows a positive peak at $X/D = -6$, revealing the influence of the upstream central jet, whereas the minimum C_P, corresponding to the g round vortex core position, is diminished substantially and occurs at $X/D = -4$ (i.e., closer to the impinging point).

Figure 9c presents the magnification of the ground static pressure distribution along the upwash zone for the three-jet case and identifies two separation points at $X/D = -7$ and -6. This result seems to be associated to the secondary recirculation zone shown in Fig. 8a, near the vertical plane of symmetry.

VI. Conclusions

Laser Doppler measurements have provided information of the mean and turbulent velocity characteristics of the fountain flows produced by two and three jets impinging on a ground plane through a confined crossflow, for $Re_j = 6 \times 10^4$ and 1.05×10^5, $V_j/U_o = 30$, and $H/D = 5$. The results show a large penetration of the impinging jets, giving rise to a ground vortex wrapped around it and developing downstream through a pair of counter-rotating streamwise vortices. The experimental results were used to validate numerical calculations of the flow based on the solution of the finite difference form of the Navier–Stokes equations, incorporating a k-ε turbulence model. The physical understanding of the flow is extended through numerical visualization of the three-dimensional nature of the ground vortex, making use of a numerical solution.

The shear layer surrounding the jets is a region of intense velocity fluctuations with maximum values located in the regions of highest mean velocity gradients. The sign of the shear stress is consistent

with the sign of the shear strain in the sense of a gradient diffusion hypothesis, with the exception of the stagnation zone associated with the formation of the ground vortex, where large effects of flow distortion on the turbulence parameters are noted.

Grid independent numerical calculations of single and multiple impinging jets flows with the k-ε turbulence model are shown to represent the gross features of the flows. The method fails to predict the turbulence structure of the impinging zone, which is not represented by the turbulent viscosity hypothesis. Also, in the ground vortex region the numerical results can be influenced by the failure of the notion of the law of the wall at separation because the flow is no longer controlled by the wall shear stress.

References

[1]Barata, J. M. M., Durão, D. F. G., and McGuirk, J. J., "Numerical Study of Single Impinging Jets Through a Crossflow," *Journal of Aircraft*, Vol. 26, No. 11, 1989, pp. 1002–1008.

[2]Knowles, K., and Bray, D., "The Ground Vortex Formed by Impinging Jets in Crossflow," AIAA Paper 91-0768, Jan. 1991.

[3]Launder, B. E., "Second-Moment Closure: Present and Future," *International Journal of Heat Transfer and Fluid Flow*, No. 10, 1989, pp. 282–300.

[4]Jones, W. P., "Turbulence Modelling: Current Practice and Future Trends," *Proceedings of the International Symposium on Engineering Turbulence Modelling and Measurement* (Dubrovnick, Yugoslavia), edited by W. Rodi and E. N. Ganic, Elsevier Science, Amsterdam, 1990.

[5]Barata, J. M. M., "Numerical and Experimental Study of Jets Impinging on Flat Surfaces Through a Crossflow," Ph.D. Thesis, Instituto Superior Técnico, Technical Univ. of Lisbon, Portugal, 1989 (in Portuguese).

[6]Saripalli, K. R., "Laser Doppler Velocimeter Measurements in 3D Impinging Twin-Jet Fountain Flows," *Turbulent Shear Flows*, edited by F. Durst, F. W. Schmidt, and J. H. Whitelaw, Vol. 5, Springer–Verlag, Berlin, 1987, pp. 147–168.

[7]Kind, R. J., and Suthanthiran, K., "The Interaction of Two Opposing Plane Turbulent Wall Jets," AIAA Paper 72-0211, Jan. 1980.

[8]Gilbert, B. L., "Detailed Turbulence Measurements in a Two Opposing Plane Turbulent Wall Jets," AIAA Paper 83-1678, July 1983.

[9]Jenkins, R. C., and Hill, W. G., Jr., "Investigation of VTOL Upwash Flows Formed by Two Impinging Jets," Grumman Research, Dept. Rept. RE-548, Bethpage, NY, Nov. 1977.

[10]Kotansky, D. R., and Glaze, L. W., "The Effects of Ground Wall-Jet Characteristics on Fountain Upwash Flow Formation and Development," ONR-CR212-216-1F, June 1980.

[11]Kavasaoglu, M. S., Schetz, J. A., and Jakubowsky, A. K., "Rectangular Jets in a Crossflow," *Journal of Aircraft*, Vol. 26, No. 9, 1989, pp. 793–804.

[12]Schetz, J. A., Jakubowsky, A. K., and Aoyagi, K., "Surface Pressures on a Flat Plate with Dual Jet Configurations," *Journal of Aircraft*, Vol. 21, No. 7, 1984, pp. 484–490.

[13]Araújo, S. R. B., Durão, D. F. G., and Firmino, F. J. G., "Jets Impinging Normally and Obliquely to a Wall," AGARD CP 308, Paper 5, 1982.

[14]Sugiyama, Y., and Usami, Y., "Experiments on the Flow in and Around Jets Directed Normal to a Crossflow," *Bulletin of the Japan Society of Mechanical Engineers*, No. 22, 1979, pp. 1736–1745.

[15]Andreopoulos, J., and Rodi, W., "Experimental Investigation of Jets in a Crossflow," *Journal of Fluid Mechanics*, Vol. 138, 1984, pp. 93–127.

[16]Shayesteh, M. V., Shabaka, I. M. N. A., and Bradshaw, P., "Turbulent Structure of a Three-Dimensional Impinging Jet in a Crossflow," AIAA Paper 85-0044, Jan. 1985.

[17]Kamotani, Y., and Greber, I., "Experiments on Confined Turbulent Jets in a Crossflow," NASA CR-2392, March 1974.

[18]Stoy, R. C., and Ben-Haim, Y., "Turbulent Jets in a Confined Crossflow," *Journal of Fluids Engineering*, No. 95, 1973, pp. 551–556.

[19]Crabb, D., Durão, D. F. G., and Whitelaw, J. H., "A Round Jet Normal to a Crossflow," *Journal of Fluids Engineering*, Vol. 113, 1981, pp. 142–153.

[20]Barata, J. M. M., Durão, D. F. G., and McGuirk, J. J., "Numerical Study of Single Impinging Jets Through a Crossflow," *Journal of Aircraft*, Vol. 26, No. 11, 1989, pp. 1002–1008.

[21]Barata, J. M. M., Durão, D. F. G., Heitor, M. V., and McGuirk, J. J., "On the Analysis of an Impinging Jet on Ground Effects," *Experiments in Fluids*, No. 15, 1993, pp. 117–129.

[22]Keffer, J. F., and Baines, W. D., "The Round Turbulent Jet in a Cross-Wind," *Journal of Fluid Mechanics*, Vol. 15, 1963, pp. 481–496.

[23]Adler, D., and Baron, A., "Prediction of a Three-Dimensional Circular Turbulent Jet in a Crossflow," *AIAA Journal*, Vol. 17, No. 2, 1979, pp. 168–174.

[24]Patankar, S. V., Basu, D. K., and Alpay, S. A., "Prediction of the Three-Dimensional Velocity Field of a Deflected Jet," *Journal of Fluids Engineering*, Vol. 99, Dec. 1977, pp. 758–762.

[25]Ramsey, J. W., and Goldstein, R. J., "Interaction of a Heated Jet with a Deflecting Stream," NASA CR-72613, 1972.

[26]Jones, W. P., and McGuirk, J. J., "Computation of a Round Turbulent Jet Discharging into a Confined Crossflow," *Turbulent Shear Flows*, edited by L. Bradbury, Vol. 2, Springer–Verlag, Berlin, 1980, pp. 233–245.

[27]Demuren, A. O., "Numerical Calculations of Steady Three-Dimensional Turbulent Jets in a Crossflow," *Computer Methods in Applied Mechanics and Engineering*, Vol. 37, No. 3, 1983, pp. 309–328.

[28]Barata, J. M. M., Durão, D. F. G., Heitor, M. V., and McGuirk, J. J., "The Turbulence Characteristics of the Single Impinging Jet Through a Crossflow," *Proceedings of the 6th Symposium on Turbulent Shear Flows* (Toulouse, France), edited by F. Durst, F. W. Schmidt, and J. H. Whitelaw, 1987.

[29]Barata, J. M. M., "Fountain Flows Produced by Multijet Impingement on a Ground Plane," *Journal of Aircraft*, Vol. 30, No. 1, 1993, pp. 50–56.

[30]Saripalli, K. R., "Visualization of Multijet Impingement Flow," *AIAA Journal*, Vol. 21, No. 4, 1983, pp. 483, 484.

[31]Melling, A., and Whitelaw, J. H., "Turbulent Flow in a Rectangular Duct," *Journal of Fluid Mechanics*,Vol. 78, 1975, pp. 285–315.

[32]Durst, F., Melling, A., and Whitelaw, J. H., *Principles and Practice of Laser-Doppler Anemometry*, 2nd ed., Academic, New York, 1981.

[33]Yanta, W. J., and Smith, R. A., "Measurements of Turbulent Transport Properties with a Laser-Doppler Velocimeter," AIAA Paper 73-0169, 1978.

[34]Launder, B. E., and Spalding, D. B., "The Numerical Computations of Turbulent Flows," *Computer Methods in Applied Mechanics and Engineering*, Vol. 19, No. 1, 1979, pp. 59–98.

[35]Leonard, B. P., "A Stable and Accurate Convective Modelling Procedure Based on Quadratic Upstream Interpolation," *Computer Methods in Applied Mechanics and Engineering*, Vol. 19, 1979, pp. 59–98.

[36]Patankar, S. V., and Spalding, D. B., "A Calculation Procedure of Heat, Mass and Momentum Transfer in Three-Dimensional Parabolic Flows," *International Journal of Heat and Mass Transfer*, Vol. 15, Oct. 1972, pp. 1787–1805.

[37]Rodi, W., " Examples of Turbulence Models for Incompressible Flows," *AIAA Journal*, Vol. 20, No. 7, 1982, pp. 872–879.

[38]Baker, O. J., "The Turbulent Horseshoe Vortex," *Journal of Wind Engineering and Industrial Aerodynamics*, Vol. 6, 1981, p. 9.

[39]Andreopoulos, J., and Rodi, W., "Experimental Investigation of Jets in a Crossflow," *Journal of Fluid Mechanics*, Vol. 138, 1984, p. 127.

[40]Chen, H. C., and Patel, V. C., "Near-Wall Turbulence Models for Complex Flows Including Separation," *AIAA Journal*, Vol. 26, No. 6, 1988, pp. 641–648.

[41]Patel, V. C., Rodi, W., and Scheurer, G., "Turbulence Models for Near-Wall and Low Reynolds Number Flows: A Review," *AIAA Journal*, Vol. 23, No. 9, 1985, pp. 1308–1319.

[42]Siclari, M. J., Migdal, D, Luzzi, T. W., Jr., Barche, J., and Palcza, J. L., "Development of Theoretical Models of Jet-Induced Effects on V/STOL Aircraft," *Journal of Aircraft*, Vol. 13, No. 12, 1976, pp. 938–944.

[43]Kotansky, D. R., "The Modelling and Prediction of Multiple VTOL Aircraft Flow Fields in Ground Effect," AGARD CP-308, Paper 16, 1982.

[44]Castro, I. P., and Bradshaw, P., "The Structure of a Highly Curved Mixing Layer," *Journal of Fluid Mechanics*, Vol. 73, 1976, pp. 265–304.

[45]Bradshaw, P., "Effects of Streamline Curvature on Turbulent Flow," AGARDograph, Vol. 169, 1973.